



Contents lists available at ScienceDirect

Journal of Biomechanics

journal homepage: www.elsevier.com/locate/jbiomech
www.JBiomech.com



Evaluation of a framework for the co-registration of intravascular ultrasound and optical coherence tomography coronary artery pullbacks



David S. Molony ^{a,*}, Lucas H. Timmins ^{a,b}, Emad Rasoul-Arzrumly ^a, Habib Samady ^a,
Don P. Giddens ^b

^a Emory University School of Medicine, Atlanta, GA 30322, USA

^b Wallace H. Coulter Department of Biomedical Engineering, Georgia Institute of Technology and Emory University, Atlanta, GA 30332, USA

ARTICLE INFO

Article history:

Accepted 25 October 2016

Keywords:

Coronary
Intravascular imaging
Dynamic programming
Hemodynamics

ABSTRACT

A growing number of studies have used a combination of intravascular ultrasound (IVUS) and optical coherence tomography (OCT) for the assessment of atherosclerotic plaques. Given their respective strengths these imaging modalities highly complement each other. Correlations of hemodynamics and coronary artery disease (CAD) have been extensively investigated with both modalities separately, though not concurrently due to challenges in image registration. Manual co-registration of these modalities is a time expensive task subject to human error, and the development of an automatic method has not been previously addressed. We developed a framework that uses dynamic time warping for the longitudinal co-registration and dynamic programming for the circumferential co-registration of images and evaluated the methodology in a cohort ($n = 12$) of patients with moderate CAD. Excellent correlation was seen between the algorithm and two expert readers for longitudinal co-registration ($CCC = 0.9964$, $CCC = 0.9959$) and circumferential co-registration ($CCC = 0.9688$, $CCC = 0.9598$). The mean error of the circumferential co-registration angle was found to be within 10%. A framework for the co-registration of IVUS and OCT pullbacks has been developed which provides a foundation for comprehensive studies of CAD biomechanics.

© 2016 Elsevier Ltd. All rights reserved.

1. Introduction

Post-mortem studies in human coronary arteries have shown that ruptured plaques are predominantly characterized by a thin fibrous cap overlying a large necrotic core (Virmani et al., 2000). These plaques, termed vulnerable plaques or thin capped fibroatheromas (TCFAs), are characterized by a fibrous cap thickness $< 65 \mu\text{m}$. Intravascular ultrasound (IVUS) can visualize deep inside the arterial wall, providing a measurement of plaque burden, and identify plaque constituents such as necrotic core through virtual histology IVUS (VH-IVUS); however, the ability of IVUS to identify true vulnerable plaques is questionable due to its limited resolution (150–200 μm) as it cannot accurately resolve thin fibrous caps. Optical coherence tomography (OCT) is a higher resolution (10 μm) imaging modality allowing for the accurate measurement of fibrous cap thickness, providing higher sensitivity for detecting TCFAs than IVUS (Fujii

et al., 2015), but the limited penetration depth of OCT does not allow for complete plaque characterization.

Wall shear stress (WSS) is understood to play a role in both plaque formation (low WSS) and plaque destabilization (high WSS) (Gijzen et al., 2013). The relationship between hemodynamics and coronary artery disease (CAD) has been separately investigated using both IVUS and OCT. Low WSS has been shown to correlate with OCT defined thinner fibrous caps (Vergallo et al., 2014), increased VH-IVUS defined necrotic core (Samady et al., 2011) and increased IVUS derived plaque burden (Stone et al., 2012). A comprehensive biomechanics based study would ideally include both modalities given their respective strengths, though in order to achieve this a robust method is required to co-register both modalities. Several clinical studies of CAD have used this dual imaging approach, assessing both plaque burden and fibrous cap thickness (Alfonso et al., 2012; Taniwaki et al., 2015; Fujii et al., 2015; Brown et al., 2015).

Achieving one to one image correspondence between the modalities is a time consuming and difficult process. Even after identifying matching images in pullbacks (longitudinal co-registration) the images must also be rotated to the correct orientation

* Corresponding author.

E-mail address: dmolony@emory.edu (D.S. Molony).

(circumferential co-registration). Given these challenges an automatic method for co-registering these modalities is of great interest. Previous work on the co-registration of IVUS/VH-IVUS and OCT has primarily focused on the fusion of the modalities into a single image. These prior methods are either completely manual (Raber et al., 2012) (using common landmarks such as side-branches or large calcifications) and/or require manual longitudinal matching of corresponding frames (Unal et al., 2006). Another study matches IVUS and OCT images by incorporating knowledge of the longitudinal position of images but does not extend the method to the co-registration of whole pullbacks (Pauly et al., 2008).

In this study we develop and implement a framework for the co-registration of IVUS and OCT images through dynamic time warping and dynamic programming algorithms. We compare the output of the algorithm to two expert readers in a cohort of mildly diseased patients. To the best of the authors' knowledge this is the first work to automatically co-register full IVUS and OCT pullbacks.

2. Methods

2.1. Patient data acquisition

Twelve patients that underwent VH-IVUS (20 MHz Eagle Eye Gold catheter, Volcano Corp.) and OCT (DragonFly C7 catheter, St. Jude) imaging were selected from our database. Patients had mild coronary artery disease with plaque burden (measured by IVUS) ranging from 18% to 53% ($\text{mean} \pm \text{stdev} = 30 \pm 11.5\%$). All imaging data were acquired during the same cardiac catheterization procedure. The IVUS pullback speed was 0.5 mm/s (~0.5 mm image spacing) and the OCT pullback speed was 20–25 mm/s (0.2–0.25 mm image spacing) with a frame rate of 100 fps. Overall there were 1680 (140 ± 45.7) VH-IVUS and 3313 (276 ± 81) OCT images. Eligible patients provided written informed consent and the Emory University Institution Review Board approved the study.

2.2. Feature selection

In order to co-register a set of images from two different modalities common features between both image sets must be identified. As outlined in Section 1 this presents a challenge for the co-registration of IVUS and OCT images given the complementary nature of these tools. The first feature we use to co-register both modalities is the lumen area. Due to the natural tapering of the vessel and presence of side-branches lumen area varies along the length of the vessel and is a good indicator of axial position. The second feature we select is the lumen eccentricity, which is measured as the distance from the lumen centroid to the

artery wall at equidistant points around the circumference. Given the limited penetration depth of OCT, comparing plaque area or thickness between both modalities is not feasible. Instead, calcifications and specifically calcification arc angle are relatively straightforward to identify in both modalities and we select this as one of our features (Fig. 1). In order to enhance these features both lumen area and lumen eccentricity include side-branches contiguous with the main vessel. Finally, under the assumption that the catheter will seek a position of minimum energy (Ellwein et al., 2011), we determined the catheter angle, as the clockwise angle between a vector from the lumen centroid to the catheter centroid and a horizontal vector at the lumen centroid (Fig. 1). As this feature is more reliable in areas of higher curvature, where the catheter is in contact with the lumen wall, the value was weighted based on the distance ratio of the catheter centroid between the lumen centroid and the lumen wall. Co-registration of the modalities must be done both longitudinally (axial direction) and circumferentially, and we address these problems separately in order to reduce computational cost.

2.3. Longitudinal co-registration

Since the IVUS and OCT pullbacks speeds are very different the regions of interest are unevenly sampled. In order to reduce computational expense we downsampled the OCT data (reduced from 3313 (276 ± 81) to 1338 (111 ± 44) images) to equal the axial resolution of the ECG-gated (automatically at the R-wave peak) IVUS data. Even after this the pullbacks are not equally sampled, due to cardiac motion. Dynamic time warping is a technique used to find an optimal alignment between two time-dependent structures $X = [x_1, x_2, \dots, x_n]$ and $Y = [y_1, y_2, \dots, y_n]$, and has previously been successfully applied for the longitudinal alignment of serial IVUS pullbacks (Alberti et al., 2013). The similarity between features is calculated by the Euclidean distance $d(i, j)$ and for the alignment of structures with m features is given as

$$d(i, j) = \sqrt{\sum_{f=1}^m (x_i^f - y_j^f)^2 + n \cdot |i - j|} \quad (1)$$

where n is a weight that penalizes non-diagonal movements, i is the i th IVUS frame and j is the j th OCT frame. The features used for longitudinal co-registration are the normalized lumen area (normalized to the maximum area of both pullbacks combined) and calcification arc length. The calcification arc length is defined as

$$\text{calcification arc length} = \left(\sum_{i=1}^{360} \text{Calc_arc}_i \right) / 360 \quad (2)$$

where Calc_arc is a binary vector indicating whether a calcification is present at each point around the lumen circumference (Fig. 1). Due to observed differences in lumen area measurement between IVUS and OCT, possibly due to incorrect OCT calibration, we apply a correction factor (with values 0.9, 1 and 1.1) to the OCT area measurement, though this could also be equally applied to the IVUS area.

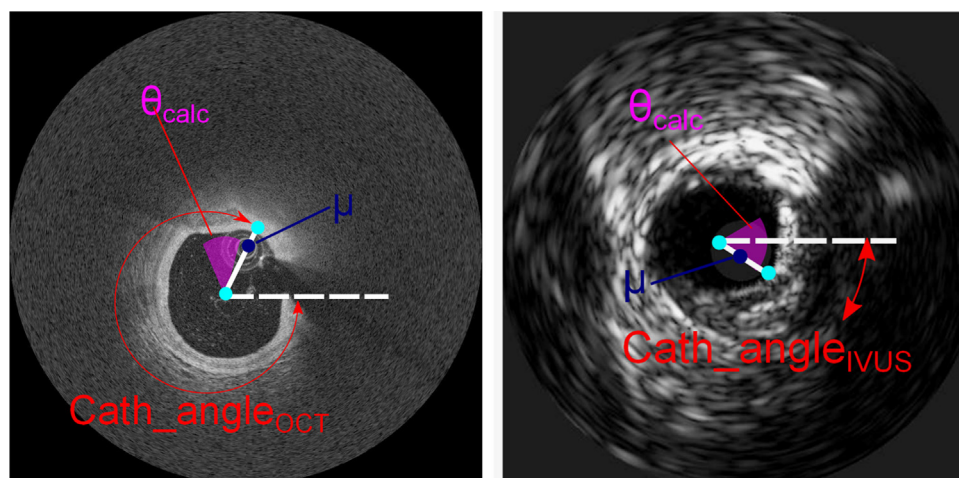


Fig. 1. Description of features used for co-registration. The blue marker indicates the position of the catheter relative to the distance between the lumen centroid and lumen wall (cyan markers) and this gives the weight μ . The value for μ in the OCT and the IVUS image are 0.8 and 0.3 respectively. Magenta indicates the calcification arc angle θ_{calc} . The catheter angles $\text{Cath_angle}_{\text{IVUS}}$ and $\text{Cath_angle}_{\text{OCT}}$ are measured clockwise from a horizontal line drawn from the lumen centroid. θ_{cath} the angle between the two catheters is given as $\text{Cath_angle}_{\text{IVUS}} - \text{Cath_angle}_{\text{OCT}}$. In the images shown $\text{Cath_angle}_{\text{OCT}}$ is 280° , $\text{Cath_angle}_{\text{IVUS}}$ is 25° while θ_{cath} is -255° . (For interpretation of the references to color in this figure legend, the reader is referred to the web version of this article.)

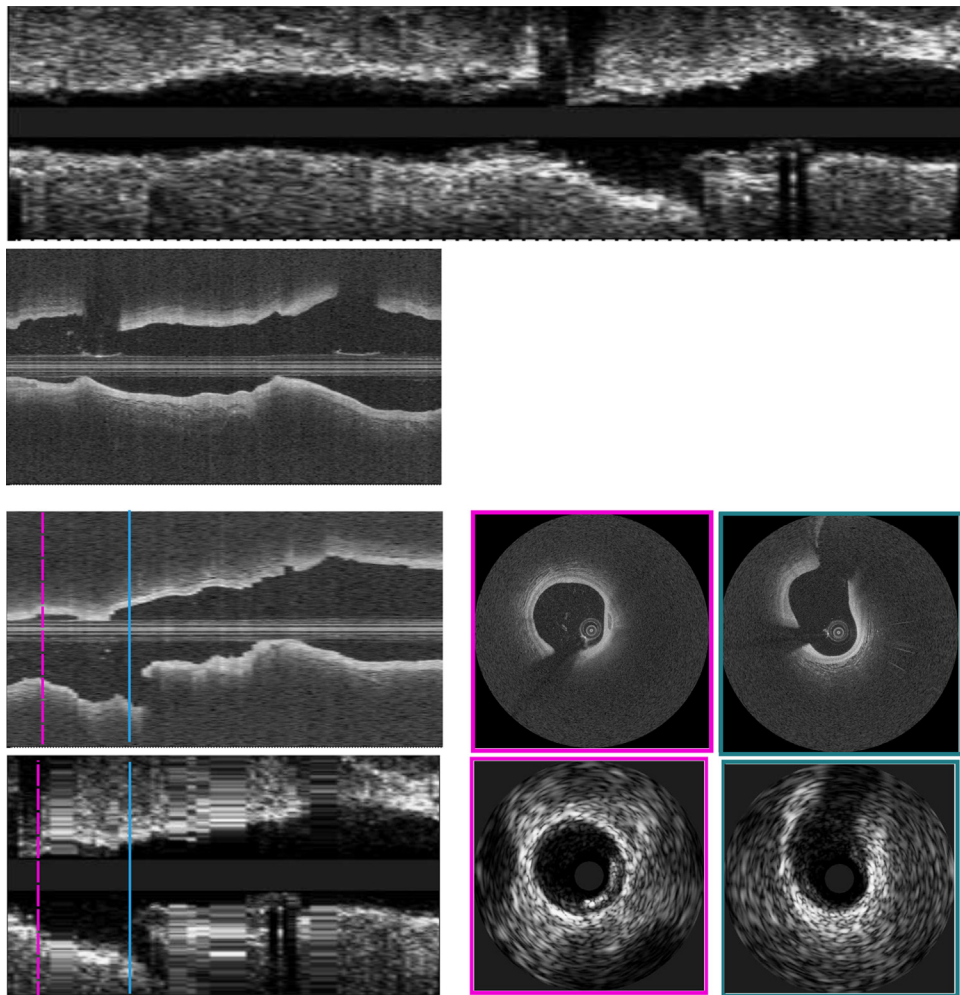


Fig. 2. Example of co-registered IVUS and OCT pullbacks. From top to bottom; initial unregistered longitudinal view of IVUS pullback; Initial unregistered longitudinal view of OCT pullback; Co-registered OCT pullback with 2 longitudinally and circumferentially co-registered images; Co-registered IVUS pullback with 2 longitudinally co-registered images. Note the correspondence between the calcification of the first image pair (magenta) and the side-branch in the second image pair (cyan).

The calculation of the minimum cumulative distance matrix D is achieved as follows

$$D(i,j) = d(i,j) + \min \left\{ \begin{array}{l} D(i-1,j), \\ D(i-1,j-1) \\ D(i,j-1) \end{array} \right\} \quad (3)$$

The matrix D is initialized with the following values

$$\left\{ \begin{array}{l} D(i,1) = D(i-1,1) + d(i,1) \\ D(1,j) = D(i,j-1) + d(1,j) \end{array} \right. \quad (4)$$

Finally, as observed in Fig. 2 the beginning (and end) of the IVUS and OCT pullbacks is almost always not at the same location. To account for this we use the sliding window approach proposed by Alberti et al. (2013). The OCT pullback is iteratively overlapped over the IVUS pullback, and the cumulative distance matrix D is calculated at each iteration. The matrix D is divided by the number of overlapped images so that shorter overlaps are not favored. The minimum overlapping number of frames is set to 25, and for each iteration the OCT pullback is displaced 10 images. This operation is performed over the range of the correction factors. The overlapping OCT and IVUS image frames with the lowest cost in the final entry of matrix D are then chosen as the best match. By backtracking from $D(x_n, y_n)$ to $D(1, 1)$ by following the minimum values we can match corresponding IVUS and OCT image frames.

2.4. Circumferential co-registration

Following image matching through the longitudinal co-registration we implement a dynamic programming framework to determine the correct rotation angle between each matched image pair. Dynamic programming is an algorithm that

finds a global optimum solution to a problem by finding the solution to sub-problems of the global problem. The algorithm will find the optimum co-registration angle between each image pair with respect to the chosen cost function. For our cost function we choose three features that vary circumferentially, namely, lumen eccentricity, calcification angle and catheter angle. The cost matrix C is given by:

$$C(i, \theta) = \alpha(1 - \text{Corr}_{ecc}(i, \theta)) + \beta(1 - \mu * \text{Corr}_{cath}(i, \theta)) + \kappa(1 - \text{Corr}_{calc}(i, \theta)) \quad (5)$$

where i is the i th IVUS image (and matched OCT image), θ is the co-registration angle between the paired images and α , β , and κ represent weights for the lumen eccentricity (Corr_{ecc}) and calcification (Corr_{calc}) are determined through normalized cross-correlation as we have previously used for the co-registration of serial VH-IVUS pullbacks (Timmins et al., 2013). In order to compute the correlation the eccentricity and calcification OCT features are rotated at 2 degree increments and the correlation for Corr_{ecc} and Corr_{calc} is given by

$$\text{Corr}(i, \theta) = \frac{1}{n-1} \sum_{r=1}^n \frac{(f(r) - \bar{f})(g(r, \theta) - \bar{g})}{\sigma_f \sigma_g} \quad (6)$$

where n is the number of increments chosen around the circumference of the image, $f(r)$ and $g(r, \theta)$ are the costs for the IVUS and rotated OCT variables in the radial direction, \bar{f} and \bar{g} are the average IVUS and OCT variables, and σ_f and σ_g are their respective standard deviations. Corr_{cath} assumes that the catheter will lie at the same angular coordinate in the lumen of both modalities so that a rotation of θ_{cath} will align the catheter in the OCT image with the IVUS image where θ_{cath} is given by

$$\theta_{cath} = \text{Cath_angle}_{IVUS} - \text{Cath_angle}_{OCT} \quad (7)$$

where Cath_angle_{IVUS} and Cath_angle_{OCT} are clockwise angles between the

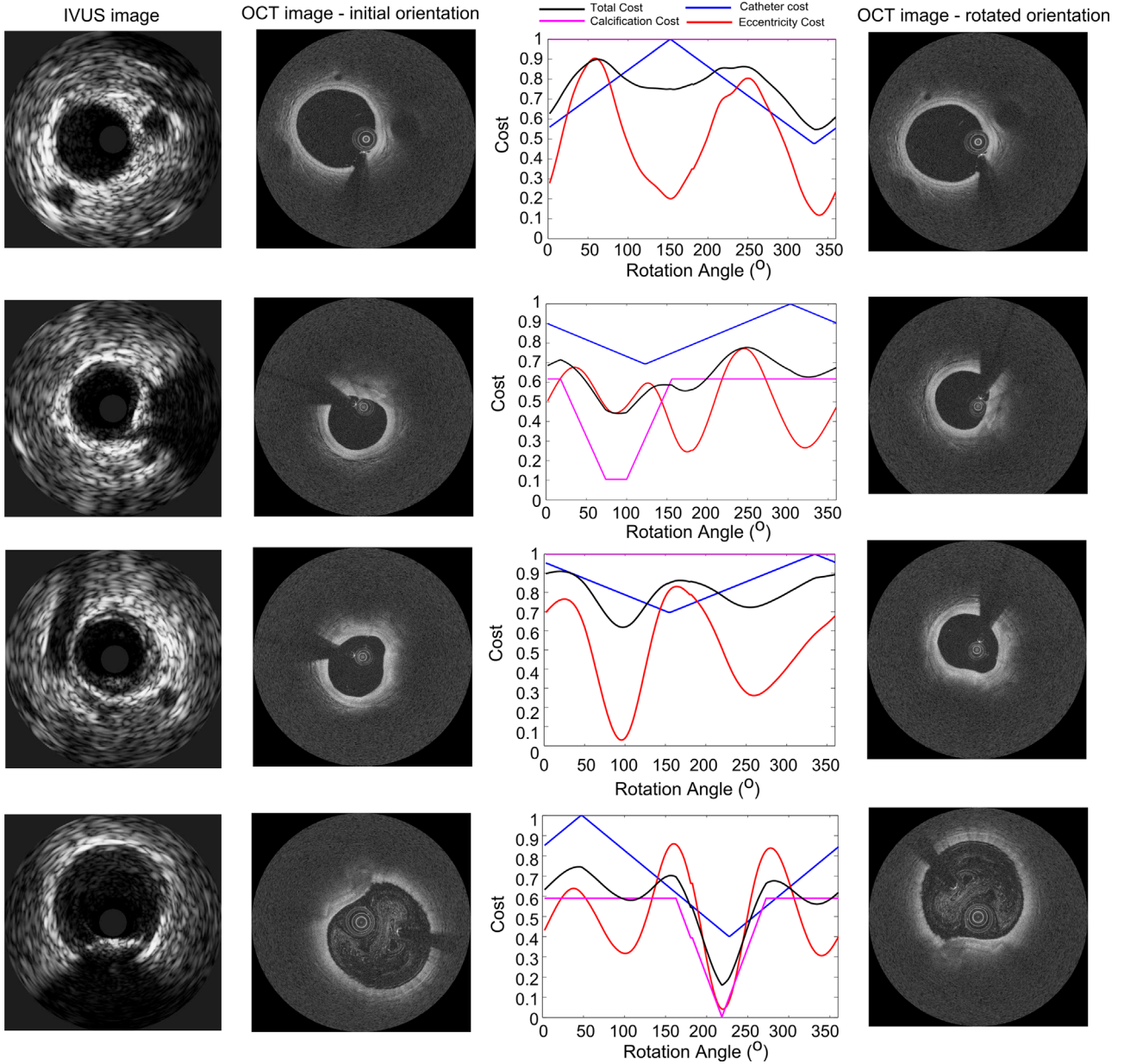


Fig. 3. Individual examples of circumferential co-registration algorithm; From top to bottom; Example where no plaque is present and the only similar feature between both examples is the catheter angle, resulting in a low catheter cost and lower total cost when the OCT image is rotated by 340°; Example where a prominent calcification is visible in both modalities, resulting in a low calcification cost at 90°; Example where the lumen eccentricity cost is low at 100°, resulting in a lower total cost at this angle; Example where all 3 features are strong resulting in individual feature low costs and a low total cost at 225°.

respective catheter centroids and a horizontal vector (Fig. 1). Under this assumption a value of 1 is prescribed at θ_{cath} and the correlation, $Corr_{cath}$, decreases away from this point so that the correlation between the catheter angles for the i th image pair is then given by

$$\begin{aligned} Corr_{cath}(i, \theta_{cath} - 180 \dots \theta_{cath}) &= \epsilon\{0 \dots 1\} \\ Corr_{cath}(i, \theta_{cath} \dots \theta_{cath} + 180) &= \epsilon\{1 \dots 0\} \end{aligned} \quad (8)$$

Due to increasing uncertainty in this feature as the catheter moves further away from the lumen wall $Corr_{cath}$ is multiplied by μ , a weight for the normalized linear distance of the IVUS catheter along a path from the lumen centroid to the artery wall. When the catheter centroid is close to the wall μ will take on a value close to 1 (Fig. 1). Examples of the co-registration features are shown in Fig. 3.

Next, we compute the cumulative cost matrix CC , as the following:

$$CC(i, \theta) = \min_{d\theta \{-\theta_{limit} \dots 0 \dots \theta_{limit}\}} \left\{ CC(i-1, \theta + d\theta) + C(i, \theta) + w \cdot \sqrt{1 + \left(\frac{d\theta}{\theta_{limit}} \right)^2} \right\} \quad (9)$$

where θ_{limit} is an angular constraint applied to prevent large angular twisting

between consecutive image pairs. The final term in the above equation is a shape constraint term introduced by Zahnd et al. (2014a) and favors closer angles to the current co-registration angle when the smoothness parameter w is set to higher values. The lowest cost path through the cumulative cost matrix is found by backtracking the path from the minimum value of the final row of CC and we constrain the path to only move within θ_{limit} . This path represents the co-registration angle between each IVUS and OCT image pairing (Fig. 4). The framework was implemented in MATLAB (MathWorks, Natick, MA, USA).

2.5. Parameter assignment

Parameters were heuristically determined on the entire dataset. For the dynamic time warping algorithm the diagonal parameter n was set to 0.003. The value of the weights for the circumferential co-registration found to have the best agreement with the expert readers was 0.5, 0.3 and 0.2 for the lumen eccentricity, catheter angle and calcification costs respectively. The angular constraint parameter θ_{limit} was set to 8° and the smoothness parameter w was set to 0.2 as this

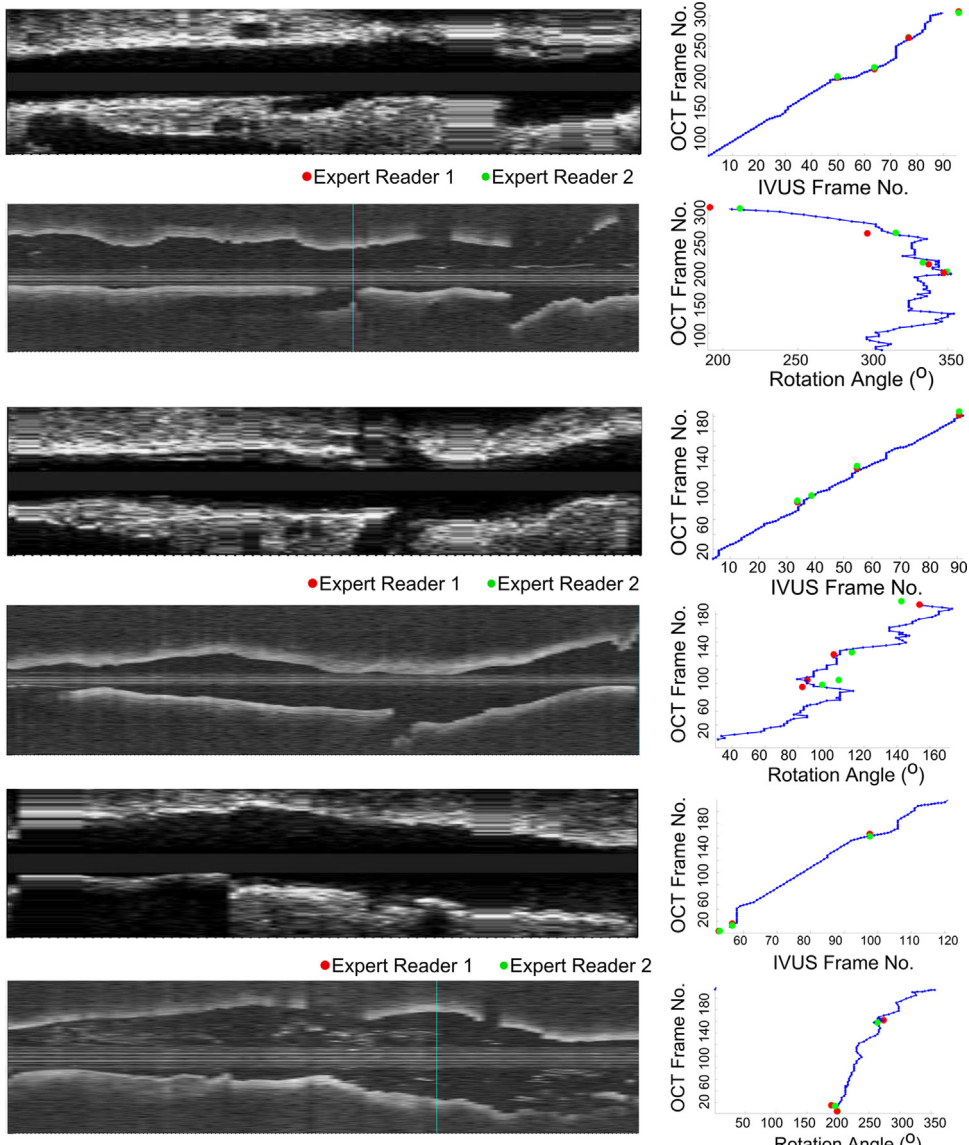


Fig. 4. Longitudinal co-registration agreement between algorithm and expert readers for all patients. Top row shows linear regression analysis and concordance correlation coefficient. Frame no. refers to the OCT frame no., chosen by either the algorithm or expert readers, which corresponds to the selected IVUS frame no. The regression and $y = x$ lines are represented by solid and dotted black lines respectively. Bottom row shows Bland–Altman plots where LoA indicates the limits of agreement.

was found to result in a smoother (without overconstraining) co-registration angle along the pullback length. Sensitivity analysis for the parameters n and θ_{limit} is included in the [Supplementary material](#).

2.6. Evaluation of pullback co-registration

Two expert readers analyzed both IVUS and OCT pullback datasets. Expert reader 1 identified IVUS landmarks (e.g., side-branches, calcified regions) and then found matching OCT images from the corresponding pullback. The IVUS landmarks were provided to expert reader 2 and the co-registration task was repeated by this reader. There are 2 types of errors associated with longitudinal and circumferential alignment of intravascular images. The first, distance error, is assessed by determining the difference in OCT frame number associated with an IVUS landmark between the algorithm and expert readers. The second, orientation error, is assessed by measuring the difference in co-registration angle between the algorithm and expert readers. Continuous data are presented as mean \pm SD and significance was determined at $p < 0.05$ with a paired t -test. Agreement between the algorithm and expert readers was assessed by calculating the concordance correlation coefficient (CCC) and Bland Altman analysis. One-way ANOVA was used for comparisons between the three groups and Tukey's post-hoc test was used for pairwise comparison. Analysis was performed using SPSS v21 (IBM Corp., Armonk, NY).

3. Results

3.1. Longitudinal co-registration

The algorithm showed strong agreement with both expert readers with CCC values > 0.99 ([Fig. 5](#)). The average difference in frames between the algorithm and the expert readers was small (Algo vs. R1: 4.4 ± 6.1 ; Algo vs. R2: 5.3 ± 6.3 ; R1 vs R2: 2.2 ± 2.3), though statistically significant ($p=0.006$). It should be noted that pairwise comparison between R1 vs. R2 and Algo. vs. R1 revealed no significant difference ($p=0.06$). The Bland–Altman analysis shows strong agreement between the algorithm and expert readers with the difference in bias between the expert readers and the algorithm being less than 1.2 frames.

Mean lumen area, normalized lumen eccentricity, normalized catheter position and calcification arc length were $11.2 \pm 3.12 \text{ mm}^2$ and $11.8 \pm 3.73 \text{ mm}^2$ ($p=0.056$); 0.87 ± 0.03 and 0.88 ± 0.02 ($p=0.55$); 0.41 ± 0.05 and 0.58 ± 0.09 ($p < 0.001$); $21 \pm 27^\circ$ and

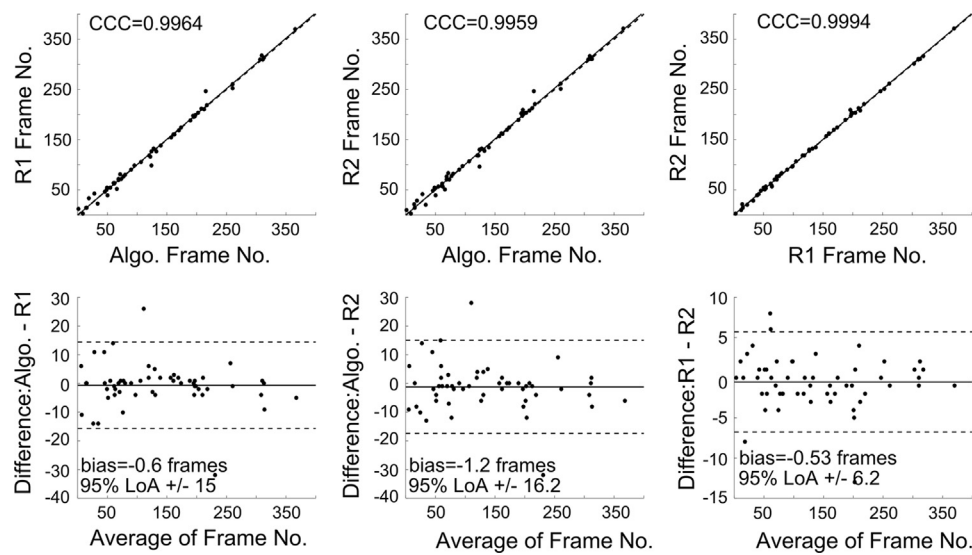


Fig. 5. Circumferential co-registration agreement between algorithm and expert readers for all patients. Top row shows linear regression analysis and concordance correlation coefficient. Co-reg angle refers to the rotation angle, chosen by either the algorithm or expert readers, applied to the OCT image to co-register it to the IVUS image. The regression and $y = x$ lines are represented by solid and dotted black lines respectively. Bottom row shows Bland–Altman plots where LoA indicates the limits of agreement.

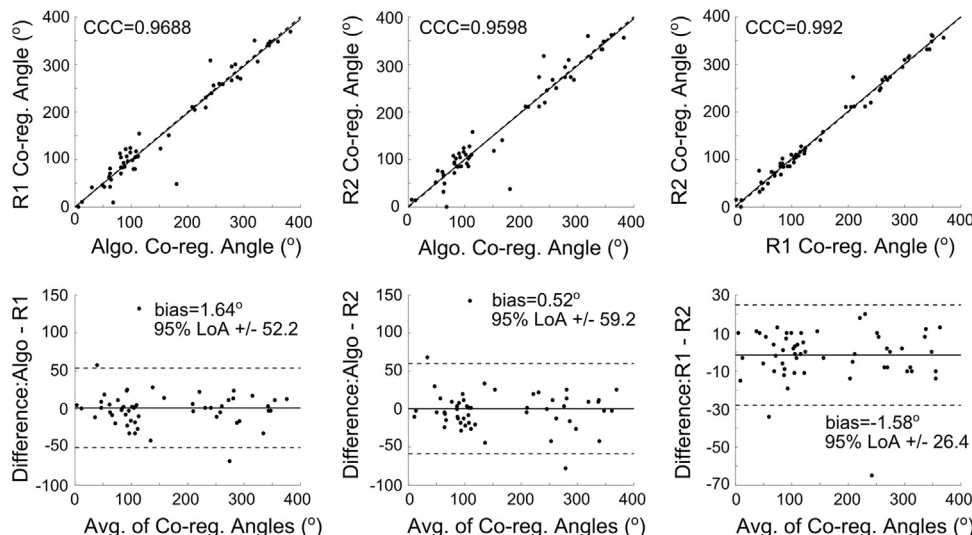


Fig. 6. Individual examples of co-registered pullbacks. Red and green markers indicate the co-registration by the expert readers while the blue path represents that of the algorithm. The last co-registered pair corresponds to IVUS images at baseline and OCT images acquired 12 months later.

$16 \pm 20^\circ$ ($p=0.046$) for IVUS and OCT images respectively. The total length of co-registered pullbacks was 49.2 ± 35.6 mm. In one case expert reader 2 could not identify the matching OCT image for the IVUS image selected by expert reader 1, while in one further case the algorithm failed to include a proximal landmark, i.e. the region co-registered by the algorithm was shorter than the manual co-registration. This also resulted in no circumferential co-registration of these images.

3.2. Circumferential co-registration

Strong agreement was seen between the algorithm and both expert readers for the co-registration angle between landmarks (Fig. 6). All CCC values were greater than 0.95 and the greatest agreement was seen between the expert readers (CCC = 0.992). Bland–Altman analysis showed no bias of the algorithm with

Table 1

Difference in number of frames and co-registration angle between the algorithm and expert readers. p -Value is derived from one-way anova for comparison between the three groups. Asterisk (*) denotes statistical significance difference for pairwise comparison with R1 and R2.

	Algo. vs. R1	Algo. vs. R2	R1 vs R2	p -Value
Frame difference	4.51	5.4*	2.2	0.006
Angle difference	16.2	19.4*	8.3	0.006

respect to either expert reader, though the 95% limits of agreement for the algorithm were twice that of the expert readers. The average difference in co-registration angle between the algorithm and expert readers (Algo vs R1: $16 \pm 20.7^\circ$; Algo vs R2: $18.8 \pm 23.1^\circ$;

R1 vs R2: $9.3 \pm 9.7^\circ$) was statistically significant ($p=0.006$). However, pairwise comparison between R1 vs R2 and Algo vs R1 was not significantly different ($p=0.067$) (Table 1).

4. Discussion

4.1. Performance of the algorithm

The correlation between the algorithm and expert reviewers was found to be very good ($CCC > 0.95$), however, a pairwise comparison revealed a significant difference between the algorithm vs. expert reader 2 and expert reader 1 vs. expert reader 2 (gold standard) for both the difference in frame number and difference in co-registration angle. The mean difference in frames corresponded to a small distance mismatch of 0.585 mm or 4.5 OCT frames (Algo. vs. R1) and 0.7 mm or 5.4 OCT frames (Algo. vs. R2). This corresponds to a small distance over a mean total co-registered pullback length of 49.2 mm. As this is the first study reporting the co-registration of IVUS and OCT pullbacks we cannot make comparisons with previous work but the error observed here compares favorably with studies that have longitudinally co-registered serial IVUS images. The mean difference in co-registration angle was 16.2° (Algo. vs. R1) and 19.4° (Algo. vs. R2) which equates to an error of approximately 10% given the range of possible co-registration angle lies between 0° and $\pm 180^\circ$. This error is larger but comparable to other co-registration studies of serial IVUS images which have reported values ranging from $7.7\text{--}9.2^\circ$ (Zhang et al., 2015) and 5.75° (Timmis et al., 2013). It should be noted that the performance of the algorithm can only be evaluated in regions where landmarks were identified by the expert reader in both modalities. Due to the lack of identifiable features present in both modalities only 56 landmarks were used for validation of the algorithm.

The algorithm was found to be faster than the expert readers. The mean algorithm computation time was 2.23 min, while the mean time for the expert readers was 8.66 min. It should be noted that the co-registration time for the expert readers only results in the co-registration of the landmark images whereas the algorithm co-registers the whole pullback. Manual co-registration of IVUS and OCT images outside of side-branch images is extremely difficult and requires estimation of the distance from a known landmark and analysis of lumen shape and configuration of calcifications over a number of frames (Raber et al., 2012). Taking all this information into account can be challenging and it is quite possible that the algorithm performs better than expert readers in these regions, though this must be validated. One possible way to validate these non-landmark images would be through IVUS and OCT imaging of phantom models or excised coronary arteries. In several co-registered frames the IVUS image was found to repeat, which may be surprising as this is ECG-gated, this could be attributed to the presence of cardiac motion in the OCT pullback where the same area may be imaged twice.

As three features are used for the circumferential co-registration the algorithm may not perform optimally in pullback regions where calcifications are not present or the catheter is positioned towards the center of the lumen. In this case only the lumen eccentricity will be reliable in predicting the correct orientation of the vessel but in vessels with concentric lumens this is not dependable. It should be noted that the majority of the patients had mild CAD. Only 2 patients from the selection had a plaque burden greater than 40% and only 5 patients had calcifications present. In a more diseased cohort features such as calcifications and lumen eccentricity would expect to exhibit stronger irregularities and hence these features would be more reliable for co-registration. The weights chosen for each feature may be biased

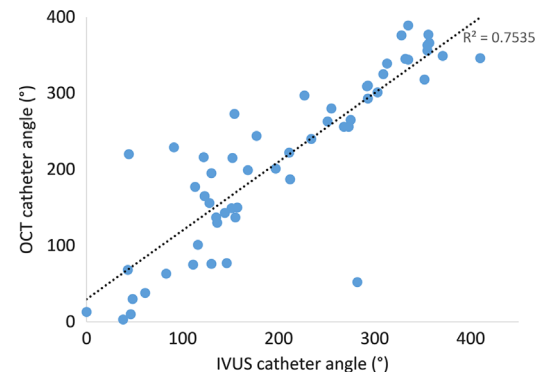


Fig. 7. Linear regression analysis between catheter angle in OCT and IVUS images where catheter angle is defined as the clockwise angle in Fig. 1. The mean angle difference was 34.8° .

towards the mildly diseased population examined here. The OCT catheter employed here is constrained within a sheath while the IVUS catheter is not. It was found that the sheathed OCT catheter (2.7F) was more often closer to the lumen wall which can be partially attributed to the larger IVUS transducer size (3.5F). To verify the accuracy of the catheter angle feature when comparing sheathed and unsheathed catheters we compared the angle in manually co-registered images (Fig. 7) and found the average difference to be 34.8° ($n=56$). The difference was found to be smaller when the catheter position was closer to the lumen wall with an average difference of 23° and 13.8° when the catheter position was greater than 0.4 ($n=35$) and 0.5 ($n=17$) respectively. The use of a sheathed IVUS catheter may result in better agreement of the catheter angle feature.

4.2. Future improvement

There are several avenues for potential improvement of the algorithm which we intend to explore in the future. The position of both the IVUS and OCT catheters is visible in angiography and may aid in co-registering the modalities (Tu et al., 2011). We chose to perform the co-registration without using this information as offline these images may not be readily available. Due to the limited penetration depth of OCT we did not attempt to use plaque thickness information in co-registering the modalities as has been successfully applied in previous co-registration studies of serial IVUS pullbacks. However, it may be possible to identify axial and circumferential regions of healthy and diseased artery in both modalities and build this feature into the algorithm (Zahnd et al., 2014b). This information could be incorporated for both the longitudinal and circumferential co-registration. Optimization of the feature weights in a broader population and adaptive weights based on the amount of eccentricity and calcification will also be explored. Future work will also investigate improving algorithm speed so that all OCT images can be used which may result in a more optimized registration.

4.3. Use of the framework for biomechanical studies of coronary artery disease

Plaque vulnerability can be quantified by simultaneously reviewing OCT observed features such as focal macrophages or fibrous cap thickness with IVUS features like necrotic core or plaque burden. The framework developed here will allow for both features to be assessed in a single patient which will help further the understanding of the biomechanics of vulnerable plaques. The circumferential co-registration of the modalities allows for focal hemodynamic associations with changes in plaque morphology to

be assessed (Molony et al., 2015; Timmins et al., 2015). This methodology can also be used to create more precise intravascular imaging-based 3D reconstructions of coronary arteries (Papafakis et al., 2015) through a combination of both modalities. Further to hemodynamic based studies it may be possible to fuse both modalities for use in structural plaque analysis. The high resolution of OCT is essential in determining the fibrous cap thickness which has been found to be the most important morphological risk factor for critical plaque stress in lesions (Akyildiz et al., 2011), while necrotic core area has also been found to be a critical feature (Ohayon et al., 2008). The developed method could also be extended for use in fluid structure interactions models (Tang et al., 2014). It should also be noted that as the framework does not depend on VH plaque information it is also fully extendable to grayscale IVUS images.

4.4. Limitations

The methodology described here requires the prior segmentation of the IVUS and OCT images as well as identification of calcifications in both modalities. While many robust automatic algorithms exist to perform these tasks (Wang et al., 2010; Zahnd et al., 2015; Balocco et al., 2014) these are imperfect and we did not test the sensitivity of the algorithm to errors in the segmentation. Image artifacts such as non-uniform rotational distortion are sometimes encountered and while this was not detected in our dataset the performance of the algorithm may be sub-optimal in the presence of such artifacts. Hybrid catheters which allow for simultaneous OCT and IVUS imaging are under ongoing development (Yin et al., 2010; Li et al., 2015). The introduction of such devices would remove the requirement of image co-registration though none of these hybrid devices are currently in clinical use.

All pullbacks in this study were collected during the same catheterization procedure and as a result the features should be very similar between both modalities. We evaluated the algorithm on one additional patient where OCT images were acquired 12 months after the original IVUS images. Despite different acquisition times for the images the algorithm performed well with a longitudinal mismatch of 2 (Algo. vs. R1) and 1.5 (Algo. vs. R1) frames and a co-registration angle error of 3° (Algo. vs. R1) and 11° (Algo. vs. R2) (Fig. 4). However, there is potential for poor algorithm performance in cases where the artery and plaque has changed significantly between timepoints. For instance, after balloon dilation or stent implantation the lumen of the vessel is likely to change. This will result in changes (and reduction in feature strength) to the lumen area and lumen eccentricity with the consequence of a weaker correlation between features of the modalities at the two different timepoints.

5. Conclusions

This study describes the first attempt to co-register whole IVUS and OCT pullbacks of coronary arteries. We introduce a framework where strong agreement in both axial and circumferential co-registration was found between the algorithm and two expert readers. The algorithm provides a faster and potentially more accurate co-registration method for studies where dual IVUS and OCT imaging has been performed and provides a foundation for a comprehensive biomechanical assessment of coronary artery disease.

Conflict of interest statement

The authors declare that no conflict of interest is associated with this paper.

Acknowledgement

This work was supported by an American Heart Association Postdoctoral fellowship (13POST17110030) and Forest Laboratories.

Appendix A. Supplementary material

Supplementary data associated with this article can be found in the online version at <http://dx.doi.org/10.1016/j.biomech.2016.10.040>.

References

- Akyildiz, A.C., Speelman, L., van Brummelen, H., Gutierrez, M.A., Virmani, R., van der Lugt, A., van der Steen, A., Wentzel, J.J., Gijssen, F., 2011. Effects of intima stiffness and plaque morphology on peak cap stress. *Biomed. Eng. Online* 10.
- Alberti, M., Balocco, S., Carrillo, X., Mauri, J., Radeva, P., 2013. Automatic non-rigid temporal alignment of intravascular ultrasound sequences: method and quantitative validation. *Ultrasound Med. Biol.* 39, 1698–1712.
- Alfonso, F., Dutary, J., Paulo, M., Gonzalo, N., Perez-Vizcayno, M.J., Jimenez-Quevedo, P., Escaned, J., Hernandez, R., Macaya, C., 2012. Combined use of optical coherence tomography and intravascular ultrasound imaging in patients undergoing coronary interventions for stent thrombosis. *Heart* 98, 1213–1220.
- Balocco, S., Gatta, C., Wahle, A., Radeva, P., Carlier, S., Unal, G., Sanidas, E., Mauri, J., Carrillo, X., Kovarnik, T., Wang, C.W., Chen, H.C., Exarchos, T.P., Fotiadis, D.I., Destrempe, F., Cloutier, G., Pujol, O., Alberti, M., Mendizabal-Ruiz, E.G., River, M., Aksoy, T., Downe, R.W., Kakadairis, I.A., 2014. Standardized evaluation methodology and reference database for evaluating IVUS image segmentation. *Comput. Med. Imaging Graph.* 38, 70–90.
- Brown, A.J., Obaid, D.R., Costopoulos, C., Parker, R.A., Calvert, P.A., Teng, Z., Hoole, S.P., West, N.E.J., Goddard, M., Bennett, M.R., 2015. Direct comparison of virtual-histology intravascular ultrasound and optical coherence tomography imaging for identification of thin-cap fibroatheroma. *Circulation: Cardiovasc. Imaging* 8, e003487.
- Ellwein, L.M., Otake, H., Gundert, T.J., Koo, B., Shinke, T., Honda, Y., Shite, J., LaDisa, J.F., 2011. Optical coherence tomography for patient-specific 3D artery reconstruction and evaluation of wall shear stress in a left circumflex coronary artery. *Cardiovasc. Eng. Technol.* 2, 212–227.
- Fujii, K., Hao, H., Shibuya, M., Imanaka, T., Fukunaga, M., Miki, K., Tamaru, H., Sawada, H., Naito, Y., Ohyanagi, M., Hirota, S., Masuyama, H., 2015. Accuracy of OCT, grayscale IVUS and their combination for the diagnosis of coronary TCFA. *J. Am. Coll. Cardiol. Cardiovasc. Imaging* 8, 451–460.
- Gijssen, F., van der Giessen, A., van der Steen, A., Wentzel, J., 2013. Shear stress and advanced atherosclerosis in human coronary arteries. *J. Biomed.* 46, 240–247.
- Li, J., Ma, T., Mohar, D., Steward, E., Yu, M., Piao, Z., He, Y., Shung, K., Zhou, Q., Patel, P.M., Chen, Z., 2015. Ultrafast optical-ultrasonic system and miniaturized catheter for imaging and characterizing atherosclerotic plaques *in vivo*. *Nat. Sci. Rep.* 5, 18406.
- Molony, D.S., Timmins, L.H., Hung, O.Y., Rasoul-Arzrumly, E., Samady, H., Giddens, D.P., 2015. An assessment of intra-patient variability on observed relationships between wall shear stress and plaque progression in coronary arteries. *Biomed. Eng. Online* 14, S2.
- Ohayon, J., Finet, G., Gharib, A.M., Herzka, D.A., Tracqui, P., Heroux, J., Rioufol, G., Kotys, M.S., Elagha, A., Pettigrew, R.L., 2008. Necrotic core thickness and positive arterial remodeling index: emerging biomechanical factors for evaluating the risk of plaque rupture. *Am. J. Physiol. - Heart Circ. Physiol.* 295, H717–H727.
- Papafakis, M.I., Bourantas, C.V., Yonetsu, T., Vergallo, R., Kotsia, A., Nakatani, S., Lakkas, L.S., Athanasiou, L.S., Naka, K.K., Fotiadis, D.I., Feldman, C.L., Stone, P.H., Serruys, P.W., Jang, I.K., Michalis, L.K., 2015. Anatomically correct three-dimensional coronary artery reconstruction using frequency domain optical coherence tomography and angiographic data: head-to-head comparison with intravascular ultrasound for endothelial shear stress assessment in humans. *Eurointervention* 11, 407–415.
- Pauly, O., Unal, G., Slabaugh, G., Carlier, S., Fang, T., 2008. Semi-automatic matching of OCT and IVUS images for image fusion. In: SPIE Medical Imaging: Image Processing, 69142N.
- Raber, L., Ho Heo, J., Radu, M.D., Garcia-Garcia, H.M., Stefanini, G.G., Moscovitch, A., Dijkstra, J., Kelbaek, H., Windecker, S., Serruys, P.W., 2012. Offline fusion of co-registered intravascular ultrasound and frequency domain optical coherence tomography images for the analysis of human atherosclerotic plaques. *Eurointervention* 8, 98–106.
- Samady, H., Eshtehardi, P., McDaniel, M., Suo, J., Dhawan, S.S., Maynard, C., Timmins, L.H., Quyyumi, A.A., Giddens, D.P., 2011. Coronary artery wall shear stress is associated with progression and transformation of atherosclerotic plaque with arterial remodeling in patients with coronary artery disease. *Circulation* 124, 779–788.
- Stone, P.H., Saito, S., Takahashi, S., Makita, Y., Nakamura, S., Kawasaki, T., Takahashi, A., Katsuki, T., Nakamura, S., Namiki, A., Hirohata, A., Matsumura, T., Yamazaki, S., Yokoi, H., Otsuji, S., Yoshimachi, F., Honye, J., Harwood, D., Reitman, M., Coskun, A.U., Papafakis, M.I., Feldman, C.L., 2012. Prediction of progression of

- coronary artery disease and clinical outcomes using vascular profiling of endothelial shear stress and arterial plaque characteristics: the PREDICTION Study. *Circulation* 126, 172–181.
- Tang, D., Kamm, R.D., Yang, C., Zheng, J., Canton, G., Bach, R., Huamg, X., Hatsukami, T.S., Zhu, J., Ma, G., Maehara, A., Mintz, G.S., Yuan, C., 2014. Image-based modeling for better understanding and assessment of atherosclerotic plaque progression and vulnerability: data, modeling, validation, uncertainty and predictions. *J. Biomech.* 47, 834–846.
- Tanuwaki, M., Radu, M.D., Garcia-Garcia, H.M., Heg, D., Kelbaek, H., Holmvang, L., Moschovitis, A., Noble, S., Pedrazzini, G., Saunamaki, K., Dijkstra, J., Landmesser, U., Wenaweser, P., Meier, B., Stefanini, G.G., Roffi, M., Luscher, T.F., Windecker, S., Raver, L., 2015. Long-term safety and feasibility of three-vessel multimodality Intravascular imaging in patients with ST-elevation myocardial infarction: the IBIS-4 (integrated biomarker and imaging study) substudy. *Int. J. Cardiovasc. Imaging* 31, 915–926.
- Timmins, L.H., Molony, D.S., Eshtehardi, P., McDaniel, M.C., Oshinski, J.N., Samady, H., Giddens, D.P., 2015. Focal association between wall shear stress and clinical coronary artery disease progression. *Ann. Biomed. Eng.* 41, 94–106.
- Timmins, L.H., Suever, J.D., Eshtehardi, P., McDaniel, M.C., Oshinski, J.N., Samady, H., Giddens, D.P., 2013. Framework to co-register longitudinal virtual histology-intravascular ultrasound data in the circumferential direction. *IEEE Trans. Med. Imaging* 32, 1989–1996.
- Tu, S., Holm, N.R., Koning, G., Huang, Z., Reiber, J.H.C., 2011. Fusion of 3D QCA and IVUS/OCT. *Int. J. Cardiovasc. Imaging* 27, 197–207.
- Unal, G., Lankton, S., Carlier, S., Slabaugh, G., Chen, Y., 2006. Fusion of IVUS and OCT through semi-automatic registration. In: Proceedings of MICCAI Workshop in Computing and Visualization for (Intra) Vascular Imaging (CVII), Copenhagen.
- Vergallo, R., Papafaklis, M.I., Yonetstu, T., Bourantas, C.V., Andreou, I., Wang, Z., Fujimoto, J.G., McNulty, I., Lee, H., Biasucci, L.M., Crea, F., Feldman, C.L., Michalis, L.K., Stone, P.H., Jag, I.K., 2014. Endothelial shear stress and coronary plaque characteristics in humans: combined frequency-domain optical coherence tomography and computational fluid dynamics study. *Circ. Cardiovasc. Imaging*, 905–911.
- Virmani, R., Kolodgie, F.D., Burke, A.P., Farb, A., Schwartz, S.M., 2000. Lessons from sudden coronary death: a comprehensive morphological classification scheme for atherosclerotic lesions. *Arter. Thromb. Vasc. Biol.* 20, 1262–1275.
- Wang, Z., Kyono, H., Bezerra, H.G., Wang, H., Gargesa, M., Alraies, C., Xu, C., Schmitt, J.M., Wilson, D.L., Costa, M.A., Rollins, A.M., 2010. Semiautomatic segmentation and quantification of calcified plaques in intracoronary optical coherence tomography images. *J. Biomed. Opt.* 15, 061711.
- Yin, J., Yang, H.C., Li, X., Zhang, J., Zhou, Q., Hu, C., Shung, K.K., Chen, Z., 2010. Integrated intravascular optical coherence tomography ultrasound imaging system. *J. Biomed. Opt.* 15, 010512.
- Zahnd, G., Orkisz, M., Serusclat, A., Moulin, P., Vray, D., 2014a. Simultaneous extraction of carotid artery intima-media interfaces in ultrasound images: assessment of wall thickness temporal variation during the cardiac cycle. *Int. J. Comput. Assist. Radiol. Surg.* 9, 645–658.
- Zahnd, G., Karanasos, A., van Soest, G., Regar, E., Niessen, W., Gijssen, F., van Walsum, T., 2014b. Fully automated detection of healthy wall sections in intracoronary optical coherence tomography. In: Proceedings of MICCAI Workshop in Computing and Visualization for (Intra) Vascular Imaging (CVII), Boston.
- Zahnd, G., Karanasos, A., van Soest, G., Regar, E., Niessen, W., Gijssen, F., van Walsum, T., 2015. Quantification of fibrous cap thickness in intracoronary optical coherence tomography with a contour segmentation method based on dynamic programming. *Int. J. Comput. Assist. Radiol. Surg.* 10, 1383–1394.
- Zhang, L., Wahle, A., Chen, Z., Zhang, L., Downe, R., Kovarnik, T., Sonka, M., 2015. Simultaneous registration of location and orientation in intravascular ultrasound pullbacks pairs via 3D graph-based optimization. *IEEE Trans. Med. Imaging* 34, 2550–2661.